

Influence of shear stress state on dynamic fracture of a glass ceramic Macor

Longhui Zhang

Department of Engineering Science, University of Oxford, Parks Road, Oxford, OX1 3PJ, UK

ARTICLE INFO

Keywords:

Ceramic
Shear failure
Dynamic
Hopkinson bar
High speed photography

ABSTRACT

The effect of shear stress on the dynamic failure of ceramic materials is not sufficiently investigated in the published literature. With the use of a bespoke split Hopkinson pressure bar, this paper presents an effort to investigate the dynamic shear compressive response of Macor, a model ceramic material with zero porosity and light weight characteristics. A cone specimen and cylindrical specimens with varying inclined angles are used to introduce the shear stress to the Macor ceramic. The dynamic failure initiation and crack propagation are monitored by the high speed photography and Digital Image Correlation techniques. It is found that the equivalent stress of Macor at the initiation of failure decreases nonlinearly with the increase of shear stress. The high speed images show that the crack originates from the minimum cross-section of the cone specimen and the obtuse angle corner of the inclined cylindrical specimens. The cracks propagate parallel to the inclined plane instead of the axial loading direction. The fractographic analysis shows the compacted zone in the shear fracture surfaces of the cone specimen and the inclined cylindrical specimens. This indicates a significant role of shear loading in the dynamic failure process of Macor.

1. Introduction

Ceramics with high strength and light weight are unique in engineering applications [1,2]. An effective design of light weight structure requires the understanding of the deformation and failure of advanced ceramic materials. As excellent thermal and electrical insulators, Macor is increasingly used in aerospace engineering [3,4], such as the thermal protection components and the electrical sensors in the control system of the aircraft engine. The Macor ceramic in service would experience complex stress states under impact loading. Studies of the dynamic shear behaviour of Macor are of considerable interest to designers.

The responses of various ceramic materials during high speed deformation were reported by Townsend and Field [5,6], Walley [7], Murray et al. [8] and Louro et al. [9]. The ceramic materials under impact experience complex shear and compressive stress states. This stimulates the studies of the dynamic failure of ceramic materials. The failure process of ceramic materials would be difficult to observe in some impact experiments such as the plate impact [8–10]. In addition, the influence of shear stress on the dynamic failure of ceramic materials is not sufficiently understood. The split Hopkinson pressure bar (SHPB) or Kolsky bar technique [11,12], with a metallic sleeve to confine the ceramic specimen [13,14], can be used to characterize the dynamic multiaxial response of ceramic materials. However, it is difficult to monitor the damage initiation and crack propagation of the confined

specimen. In addition, the increase of confining pressure reduces the shear stress applied to the ceramic specimen. Consequently, specific shear testing techniques would be required to study the dynamic shear failure of ceramic materials.

In the last several decades, a series of shear testing techniques were developed by using different specimens, i.e., torsion specimen [15], hat-shaped specimen [16], inclined specimen [17], cone specimen [18] and shear compression specimen (SCS) [19,20]. These specimens are suitable for characterizing the dynamic shear failure of metallic alloys, see the recent use of SCS reported by Zhang et al. [21,22] and the recent use of torsion specimen reported by Zhang et al. [23]. However, due to the complexity and difficulty in machining the torsion specimen, the SCS and the hat-shaped specimen from ceramic materials, the cone specimen [18] and the inclined specimen [17] are adopted in this work to apply the shear stress to the Macor ceramic. The Hertzian cone was found in a range of ceramic materials under high speed impact, see Townsend and Field [5,6]. Studying the dynamic response of the cone specimen would be of particular interest. The Macor specimens are loaded by the SHPB synchronized with a high speed camera. The high speed camera is used to capture the dynamic failure initiation and crack propagation of the Macor specimen. Digital Image Correlation (DIC) is a popular non-contact technique for the full field strain or displacement measurement [24–26]. Here, the DIC is used to assist in the observation of the strain field of the Macor specimen. Section 2 introduces the material,

E-mail addresses: lhzhang.mechanics@gmail.com, longhui.zhang@eng.ox.ac.uk.

<https://doi.org/10.1016/j.ceramint.2022.05.102>

Received 19 March 2022; Received in revised form 30 April 2022; Accepted 9 May 2022

Available online 13 May 2022

0272-8842/© 2022 The Author. Published by Elsevier Ltd. This is an open access article under the CC BY-NC-ND license (<http://creativecommons.org/licenses/by-nc-nd/4.0/>).

Table 1
Compositions of the Macor ceramic.

Composition	F	B ₂ O ₃	K ₂ O	Al ₂ O ₃	MgO	SiO ₂
Weight (%)	4	7	10	16	17	46

specimens and experimental methods. Section 3 reports the experimental results. Section 4 discusses the main outcomes of this work, followed by the conclusion.

2. Material and methods

2.1. Material and specimens

As a white color and porcelain-like ceramic composite made by Corning Inc, Macor comprises 45% borosilicate glass and 55% fluorophlogopite mica phase. The compounds of Macor from the manufacturer [27] are given in Table 1. This ceramic has a low density of 2.52 g/cm³ with zero porosity. Fig. 1a shows the 4 mm diameter and 4 mm length

cylindrical specimen. This specimen is for the uniaxial compression test. Fig. 1b and c present the cone specimen and the cylindrical specimens with inclined angles (α) of 4° and 8°. They are used to introduce the shear stress to the Macor ceramic. The dimensions of the cone specimen and the inclined cylindrical specimen are shown in Fig. 1d–e. A minimum of 5 specimens were tested for each type of specimen. The Macor specimens were manufactured along the axial direction from the supplied material rod, using the standard carbide tool. The ends of the specimen were machined with high parallelism geometric tolerance. The specimen surfaces were mechanically polished to reduce the surface defects.

2.2. Experimental setup

Originally developed by Hopkinson [11] and modified by Kolsky [8], the SHPB has been an important technique to characterize the dynamic flow of metallic materials [28,29]. When the SHPB technique is adopted for the ceramic materials, extra care and some modifications are required to achieve a desirable dynamic loading condition [30–33].

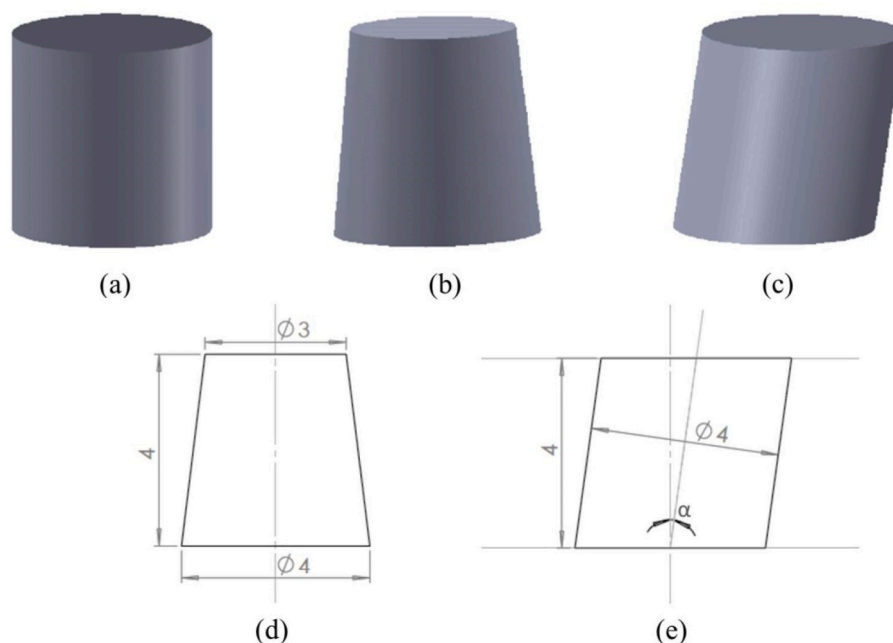


Fig. 1. Three dimensional models of (a) cylindrical specimen, (b) cone specimen (c) inclined cylindrical specimen. The dimensions of the cone specimen and the inclined cylindrical specimen are provided in (d) and (e). (unit: mm).

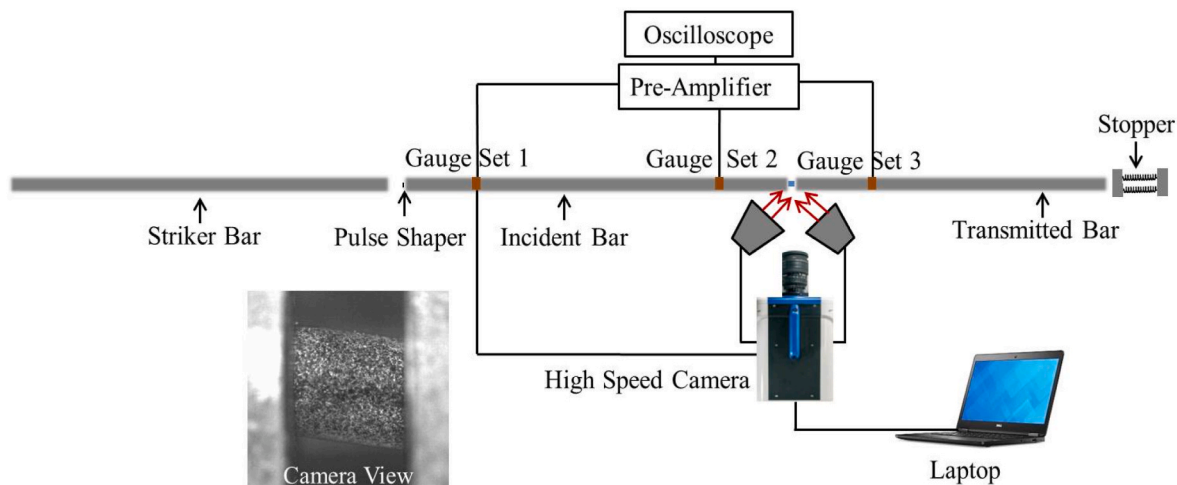


Fig. 2. Schematic Diagram of the current SHPB setup.

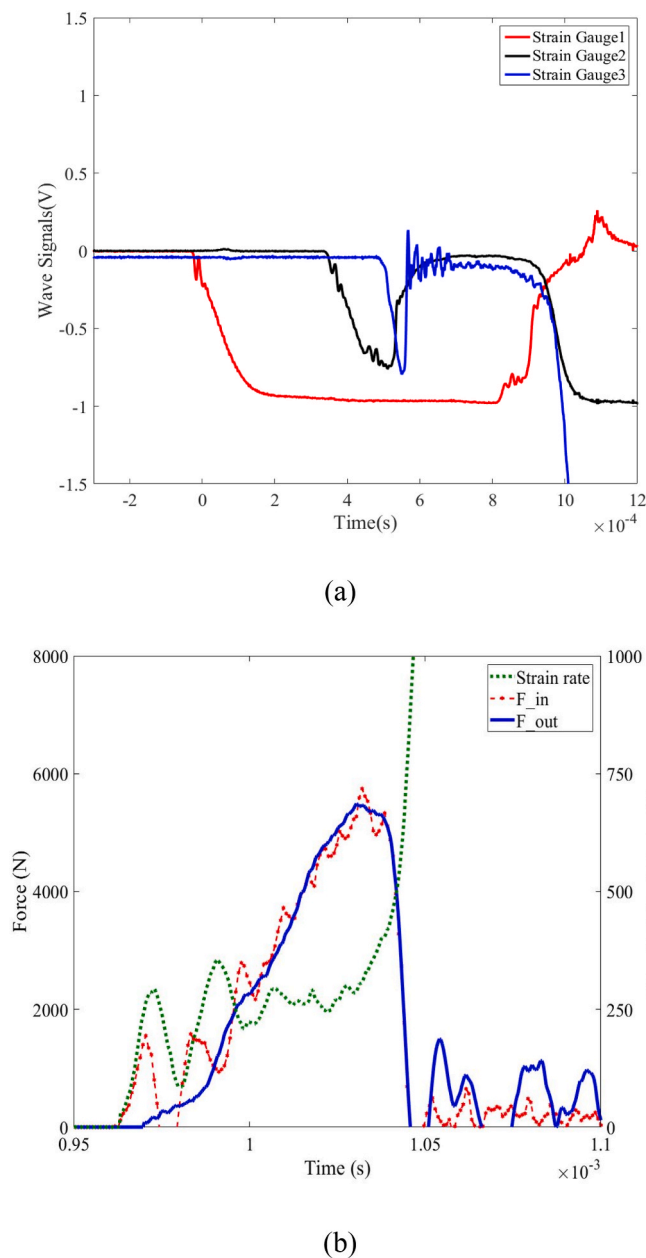


Fig. 3. Typical SHPB measurements (a) Strain gauge signals (b) Dynamic force equilibrium.

Fig. 2 presents the schematic of the SHPB setup in this work. The incident bar, transmitted bar and the striker were made from Ti6Al4V alloy. The length of the incident bar and the transmitted bar was equal to 2.7 m. The stress pulse was generated by a 2.5 m striker bar. Although this long Hopkinson bar was initially designed to test ductile materials under large deformation, this system has recently been used for the dynamic testing of brittle materials, see the works of Koen et al. [34] and Zhang et al. [35,36]. A pulse shaper, which was made from a neoprene rubber sheet with a thickness of about 0.7 mm, was attached at the impact end of the incident bar. The pulse shaper increases the rise time of the incident wave and would enable the force equilibrium of the ceramic specimen. The compression tests of the Macor specimens were performed at strain rates of about 300–500/s. The deformation and failure of Macor were monitored by a high speed camera (Specialised Imaging Kirana camera) with an image resolution of 924×748 pixels, at a framing rate of 5×10^5 fps with a shutter speed of 2 μ s. The slightly lubricated specimen is sandwiched between the incident bar and the

transmitted bar, as can be seen from the camera view in Fig. 2. The high speed photographs were processed by commercial DIC software (Lavision Davis). The matching of the images was based on a 6th order spline sub-pixel image interpolation scheme and an affine shape function [37].

In Fig. 2, one can find that two strain gauge sets (1 and 2) are placed on the incident bar, while one strain gauge set 3 is on the transmitted bar. Two strain gauge sets on the incident bar are used to separate the superimposition of the stress waves generated by the long striker bar. Analysis of the stress wave propagation can be found in Zhang et al. [35]. The measurements of the stress and strain can be obtained via the classical Hopkinson bar analysis [38]. Fig. 3a shows the typical stress wave signals of a cylindrical specimen. With the use of pulse shaper, the rise time of the incident wave is about 200 μ s. Fig. 3b compares the forces at the input side and the output side. Except for an initial oscillation [39], the force equilibrium of the specimen is achieved. The strain rate history shows an almost constant value of about 300/s during dynamic deformation. The sudden increase of strain rate indicates the loss of load bearing capacity of Macor.

3. Results

3.1. Experimental results

3.1.1. Cylindrical specimen

Fig. 4a shows the engineering stress history of the cylindrical

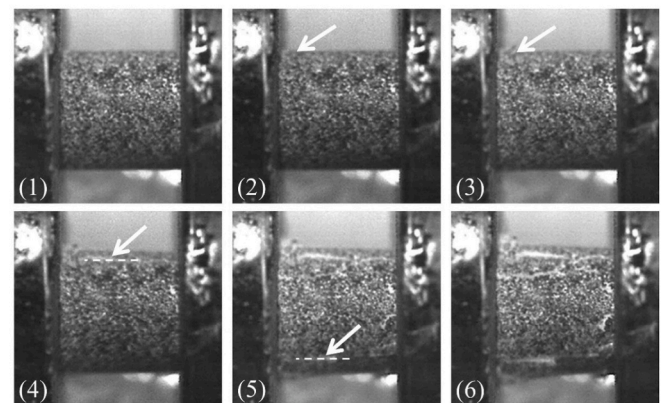
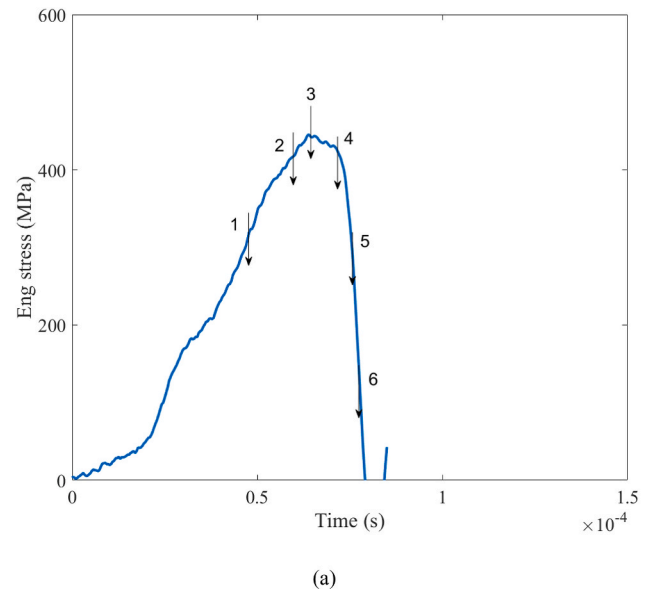


Fig. 4. Dynamic deformation of the cylindrical specimen (a) Engineering stress history (b) Deformation and failure at different stages.

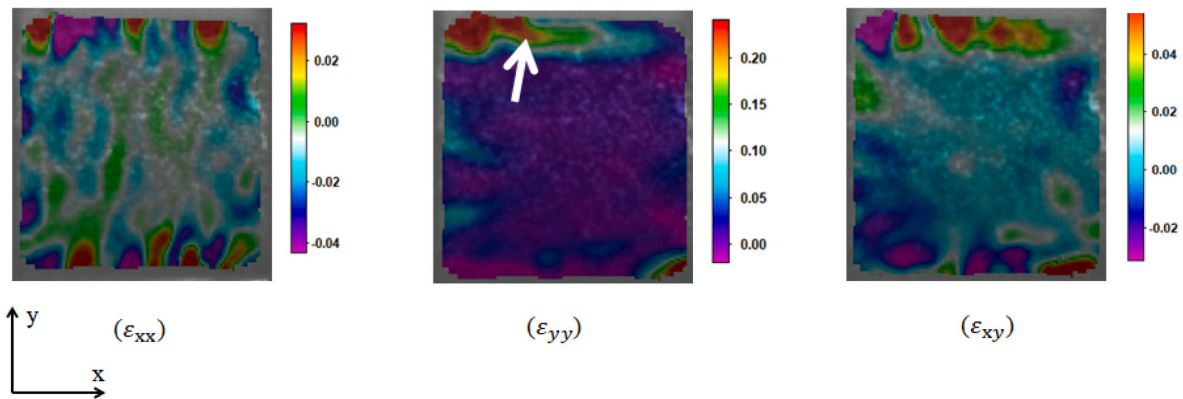
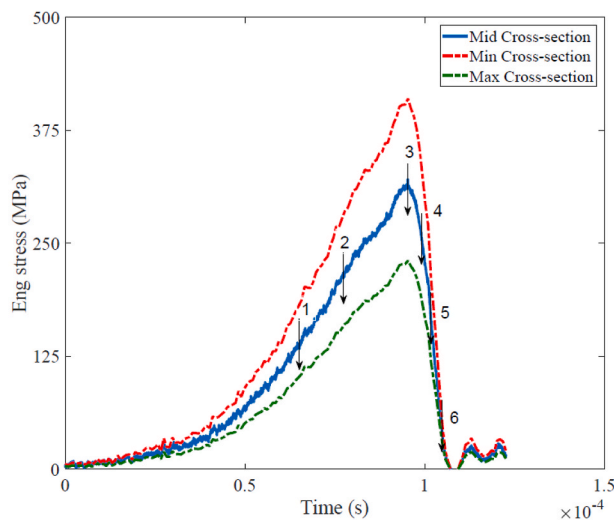
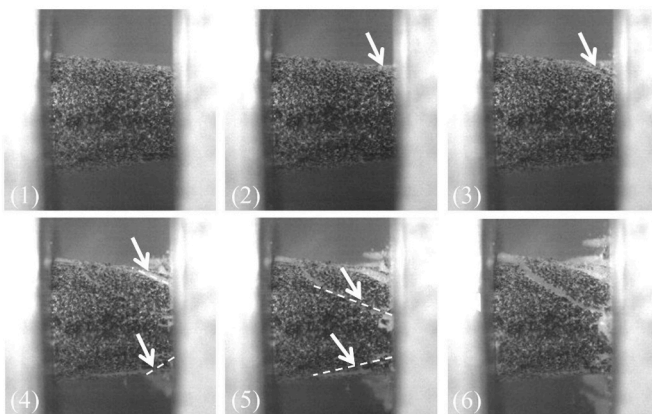


Fig. 5. Contours of compressive, tensile, and shear strain of the cylindrical specimen.



(a)



(b)

Fig. 6. Dynamic deformation of the cone specimen. (a) Stress histories at different cross-sections (b) Deformation and failure at different stages.

specimen. Fig. 4b provides the corresponding high speed images at different stages. The failure (white arrow) initiates from a small area close to the left top edge at stage 2. This indicates a tiny surface crack already appears before the stage of peak stress. The stress continues to increase to the peak stress at stage 3. The crack (dash line) propagates along the axial loading direction at stage 4. The cracks are also observed

at the bottom of the specimen at stage 5, followed by the potential fragmentation at stage 6.

Fig. 5 presents the DIC strain fields of the cylindrical specimen between stage 4 and stage 5. The failure originates from the left top edge, followed by the axial splitting. This can be observed from the tensile strain distribution (marked by an arrow). The DIC analysis also shows the failure mode of Macor with the radial expansion under dynamic compressive loading condition.

3.1.2. Cone specimen

The cone specimen was a technique initially used by Wei et al. [18] to investigate the dynamic shear failure of tungsten alloys. Townsend and Field [5,6] reported the formation of Hertzian cone in various ceramic materials under impact. The cone specimen is of particular interest in the present work. Fig. 6a compares the engineering stress histories at the maximum cross-section, mid cross-section and minimum cross-section from a dynamic test of Macor cone specimen. The minimum cross-section of the cone specimen shows a maximum stress. The high speed images in Fig. 6b show that a small crack (arrowed) initiates close to the top corner of the minimum cross-section at stage 2. Beyond the peak stress at stage 3, another crack forms at the bottom of the minimum cross-section at stage 4. The cracks propagate to the centre at stage 5, parallel to the inclined surface of the cone specimen. This is followed by the fragmentation at stage 6.

Fig. 7 presents the strain contours of the cone specimen from the test shown in Fig. 6. The failure initiates from the top corner at the minimum cross-section, followed by the splitting of the specimen (marked by the white arrows). The expansion direction is along the inclined surface direction of the cone specimen. This is different from that of the cylindrical specimen.

3.1.3. 4° and 8° inclined cylindrical specimens

The inclined cylindrical specimen was initially developed by Meyer et al. [16] to study the dynamic shear failure of metallic alloys. Here, the 4° and 8° inclined cylindrical specimens were tested using the SHPB, to investigate the influence of shear stress on the dynamic failure of Macor. The inclination introduces the shear stress to the specimen. Fig. 8a shows the average stress history of the 4° inclined cylindrical specimen. As can be seen from the high speed images in Fig. 8b, the damage initiates from the top right corner of the specimen at stage 2. Beyond the peak stress and with the continuous deformation, the failure can also be observed at the centre of the specimen at stage 5. The cracks propagate along the inclined direction of the specimen.

Fig. 9 presents the corresponding strain contours of the 4° inclined cylindrical specimen before the final fracture. It is found that the failure initiates from the top right corner of the specimen. This is followed by the splitting of specimen, as indicated by the tensile strain distribution (arrowed). Subsequently, the radial expansion occurs under the dynamic

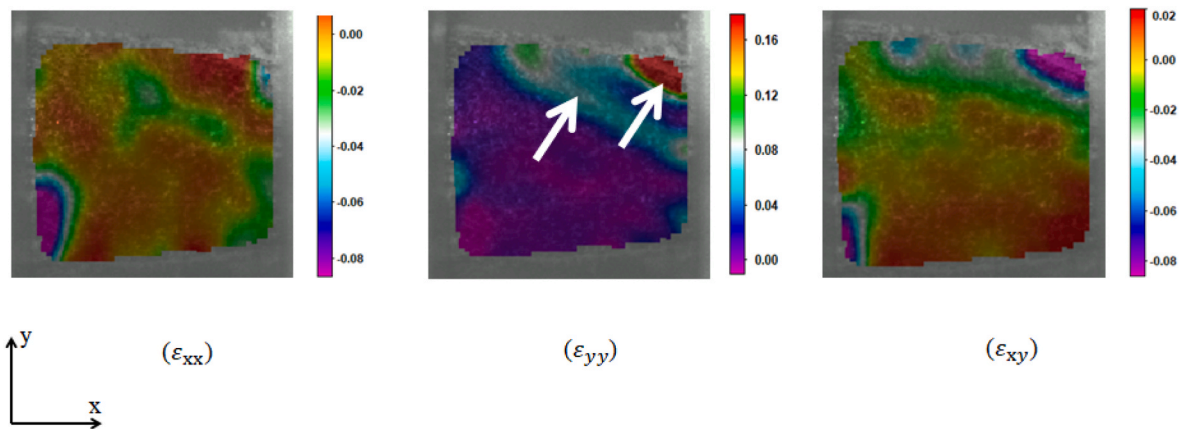
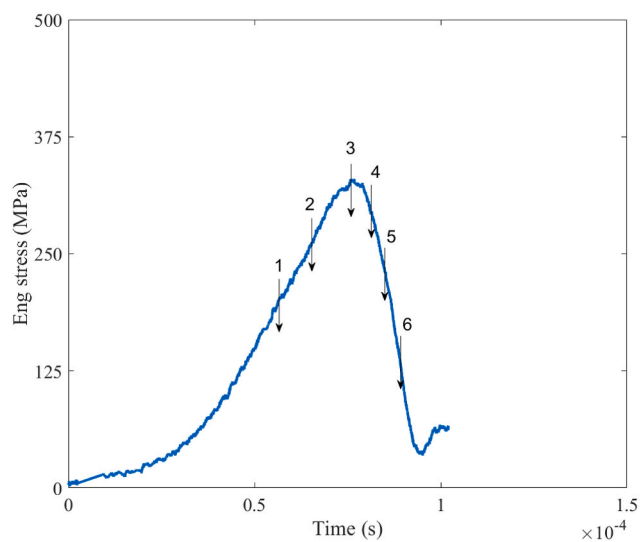
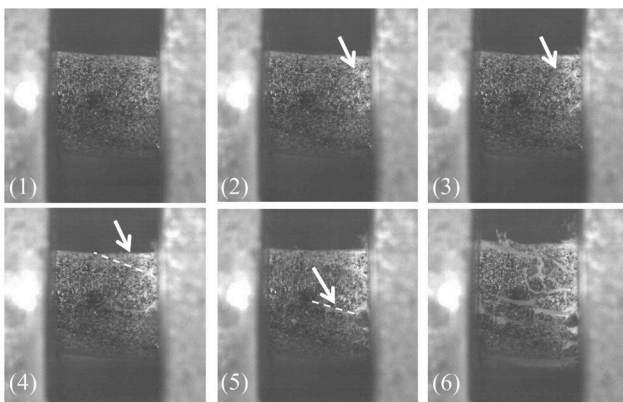


Fig. 7. DIC strain fields of the cone specimen.



(a)



(b)

Fig. 8. Dynamic deformation of the 4° inclined cylindrical specimen (a) Engineering stress history (b) Deformation and failure of the specimen at different stages.

shear compressive loading condition.

Fig. 10a presents the average stress history of the 8° inclined cylindrical specimen. As shown in Fig. 10b, the damage originates from the top right corner of the specimen at stage 2. The failure starts earlier in

the 8° inclined specimen than that in the 4° inclined specimen. Note that the stress in Fig. 10a is the average stress measured from the transmitted strain gauge signal. The local stress at the corner would be higher than this global stress value. This results in the failure initiation at the corner. When the material fails at the corner, other parts of the specimen are still at lower stress values. The failure can also be observed at the centre of the specimen at stage 5. Similar to the 4° inclined specimen, the cracks propagate along with the inclined surface direction instead of the axial loading direction.

3.2. Fractographic analysis

Fracture surfaces of the broken cylindrical specimen, the cone specimen and the inclined cylindrical specimens are characterized by the Scanning Electron Microscope (Carl Zeiss Evo LS15 VP). For the cylindrical specimen with axial splitting failure, Fig. 11a shows the fracture surface consisting of the short fiber-like mica phases (circle) and the smooth cleavage planes (dashed arrow). The transgranular fractured and randomly oriented mica phases and the cleavage planes are typical failure mechanisms of the fluorophlogopite glass ceramic [14,40,41]. For the cone specimen, Fig. 11b shows the mica phase-cleavage plane zone and compacted zone (marked by an arrow). Such a similar compaction zone was observed in the fracture surface of ceramics under punch shear loading [42], due to the abrasion of shear planes. Fig. 11c-d shows the same comminuted zone in the shear fracture surfaces of the inclined cylindrical specimens, indicating that the shear loading affects the dynamic failure process of Macor.

3.3. Finite element simulation

The global stress history measured from the transmitted pulse cannot reflect the local stress states of the inclined cylindrical specimen and the cone specimen. To obtain the equivalent stress at the initiation of failure, the local stress states need to be analysed. Here, a commercial software ABAQUS [43] is used to determine the local stress of the inclined specimen and the cone specimen, based on the SHPB analysis and the high speed photographs.

Fig. 12 shows a typical finite element model of the inclined specimen and the end of the bars. Instead of simulating the 2.7 m long incident and transmitted bars, a 3 mm length Ti6Al4V anvil is used to represent the end of the Hopkinson bars in contact with the specimen, in order to reduce the simulation time. The anvils and the specimen are meshed with three-dimensional linear hexahedral elements with default hour-glass control (reduced integration element C3D8R). The anvil is meshed with a size of 0.5 mm. The centre of the specimen is meshed with a size of 100 μm. A finer mesh with a characteristic length of 50 μm is applied at the ends of the specimen. Note that this fine mesh size is comparable

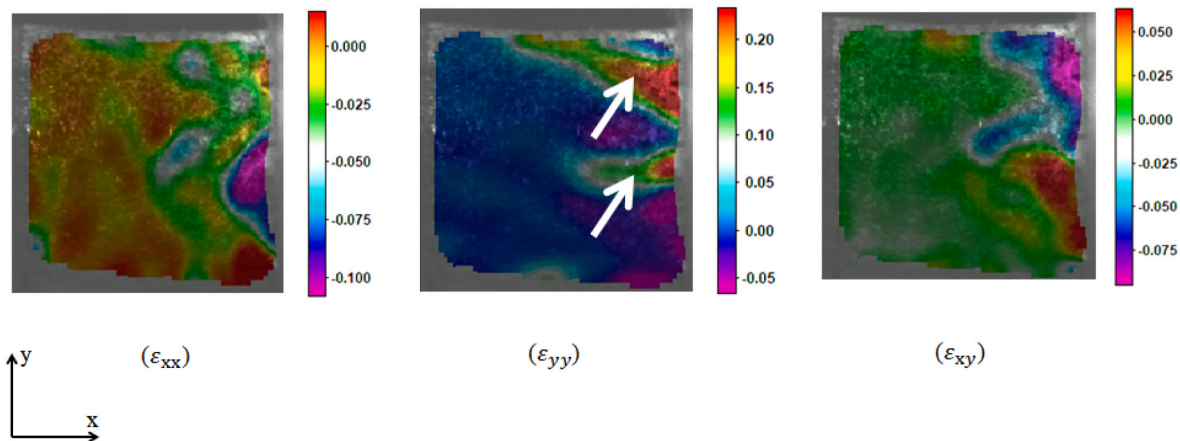
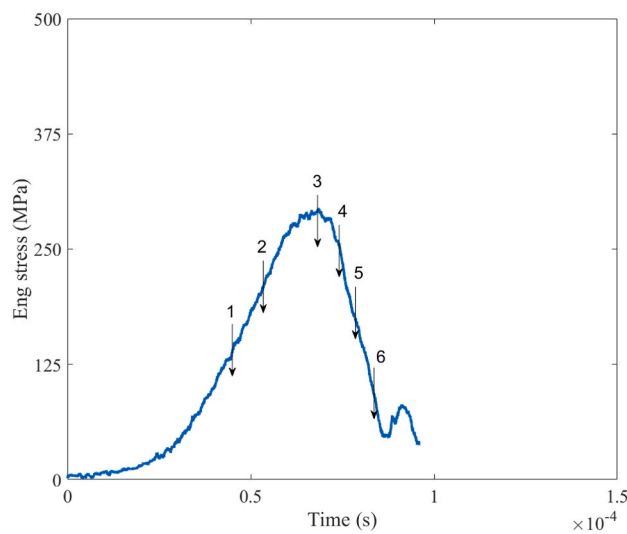
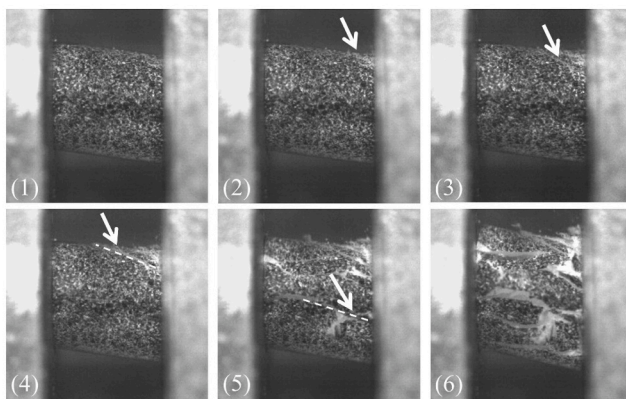


Fig. 9. DIC strain fields of the 4° inclined cylindrical specimen.



(a)



(b)

Fig. 10. Dynamic deformation of the 8° inclined cylindrical specimen. (a) Engineering stress history (b) Deformation and failure of the specimen at different stages.

to the size of fluorophlogopite mica phase of Macor. The mesh convergence was assessed, in which the output force and stress evolutions against mesh density were converged satisfactorily with the difference

of less than 1%. With a fixed bottom anvil, the experimentally measured relative velocity is used as the applied boundary condition on the top anvil and subsequently to load the specimen. Since the equivalent stress at the damage initiation is the main concern in this work, the Macor ceramic is regarded to obey the linear elastic response with Young's modulus of 60 GPa and Poisson's ratio of 0.29 [27]. More sophisticated models of ceramic materials, such as Johnson–Holmquist-II (JH-2) and phase-field model, can be found in Refs. [44–47]. The Ti6Al4V anvils are modelled with the standard linear elastic parameters [48], Young's modulus of 110 GPa, Poisson's ratio of 0.33 and Density of 4500 kg/cm³. A frictionless contact condition is assumed between the lubricated specimen and the end of the Hopkinson bars [49,50]. The chosen elements for the analysis of local equivalent stress are along a 300 μm length path [20] at the corner of the specimen, which corresponds to the failure initiation zone observed in the high speed images. The average local equivalent stress is determined as the equivalent strength of the specimen at the initiation of failure.

Fig. 13 shows the typical equivalent stress contours of the 8° inclined cylindrical specimen and the cone specimen. A first observation is that, the von Mises stress is not distributed homogeneously in these specimens. Specifically, the stress contour of the 8° inclined cylindrical specimen shows rotational symmetry about the midpoint. The higher stress values exist at the two obtuse angle corners. For the cone specimen, the stress contour is symmetrical along the axis. The higher stress values exist at two corners at the minimum cross-section.

Fig. 14 introduces the procedure to obtain the equivalent stress at the initiation of failure. Specifically, Fig. 14a shows a typical experimental force history of the 8° inclined cylindrical specimen from the Hopkinson bar analysis, together with the numerical reaction force as a function of time. The numerical force agrees well with the experimental force. With the assistance of high speed photography, the time at the initiation of failure can be determined. Fig. 14b plots the equivalent stress and the shear stress at the obtuse corner of the specimen. Corresponding to the time at the initiation of failure, the equivalent stress and shear stress of the Macor specimen can be obtained.

Fig. 15 shows the equivalent stress at the failure initiation as a function of shear stress. The average values of the equivalent stress and shear stress are given, together with the corresponding standard error. They are normalized by the uniaxial (equivalent) stress of the cylindrical specimen at the initiation of failure. In the present work, different shear stress states are applied to Macor with the use of different specimens. In Fig. 15, the normalized shear stress values increase from 0 to 5.3%. These are achieved by using the cylindrical specimen, 4° inclined cylindrical specimen, 8° inclined cylindrical specimen and the cone specimen. The increase of shear stress reduces the equivalent stress of the Macor ceramic at the initiation of failure. The nonlinear trend can be described by a second order polynomial curve. A shear stress, which is

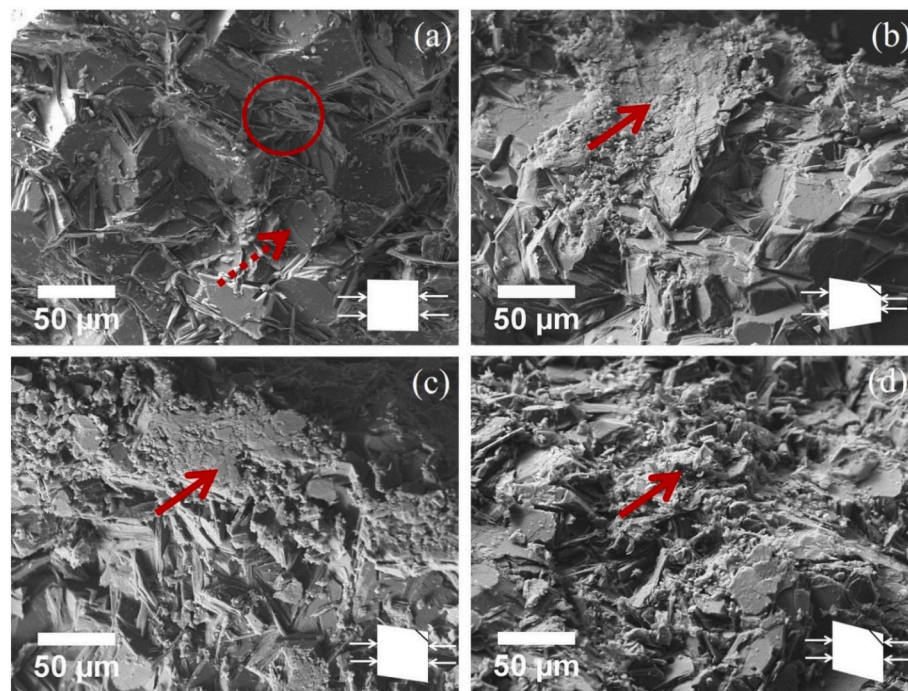


Fig. 11. Fracture surfaces of Macor under impact (a) Cylindrical specimen (b) Cone specimen (c) 4° inclined cylindrical specimen (d) 8° inclined cylindrical specimen.

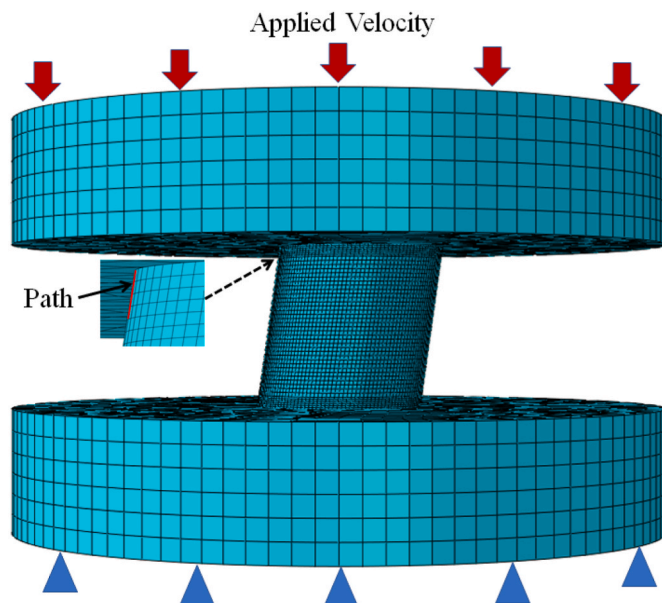


Fig. 12. Typical finite element model of the Macor specimen (8° inclined cylindrical specimen) and the ends of the bars.

only about 5% of the equivalent stress of the cylindrical specimen, results in a decrease of over 20% of the equivalent stress of the Macor ceramic at the initiation of failure. In addition, it is found that the 8° inclined cylindrical specimen and the cone specimen show comparable equivalent stress values at similar shear stress values.

From the high speed images in Figs. 6, Figs. 8 and 10, the cracks propagate to the centre of the cone and inclined specimens, roughly parallel to the inclined surface direction. Fig. 16 schematically shows the crack propagations (dashed lines) of the inclined cylindrical specimen and the cone specimen. For the 4° or 8° inclined cylindrical specimen, Fig. 16a presents that the splitting starts from the obtuse angle corner.

This is followed by the crack propagation along the inclined plane direction in Fig. 16b. For the cone specimen, the cracks firstly appear from the two corners at the minimum cross-section, followed by the propagation parallel to the inclined surface, as shown in Fig. 16c-d.

4. Discussion

This paper studies the dynamic shear compressive response of a model ceramic Macor. With the use of pulse shaping technique and the lubrication at the specimen/Hopkinson bar interfaces, the Macor specimen deforms at a constant strain rate under force equilibrium condition. For the cylindrical specimen subjected to uniaxial compressive loading, the peak stress value agrees with the results of Chen and Ravichandran [13,51]. In addition to the global force or stress measurement, the high speed photograph shows that the failure initiates before attaining the peak stress [44,52]. As a machinable ceramic with mica-glass interlocked phases [53,54], the load bearing capacity of Macor can be maintained. Later, the stress continues to increase to the maximum stress, in spite of the appearance of a tiny crack before the stage of peak stress.

For the cylindrical specimens with 4° or 8° inclined angle, the damage originates from the obtuse angle corner. Although the average engineering stress can be measured from the transmitted strain gauge signal, the stress distribution is not uniform in the inclined cylindrical specimen. The local stress at the obtuse angle corner is higher than the overall stress of the specimen. After the initiation of failure, the cracks propagate toward the areas with lower stress values. The crack propagation is along the inclined surface instead of the loading direction. This is different from the axial splitting of the cylindrical Macor specimen under uniaxial loading condition (see the wing crack propagation analysis of Chen and Ravichandran [51]). This observation agrees with that of borosilicate glass [50] or rocks [55] in the literature. The cone specimen [18] is less used for ceramic materials. Here, the shear compressive behaviour of Macor is also characterized using the cone specimen. The failure initiates from the corner at the minimum cross-section, as can be seen in Fig. 6. This is similar to the failure initiation of tungsten alloy [18]. The combined shear compressive stress

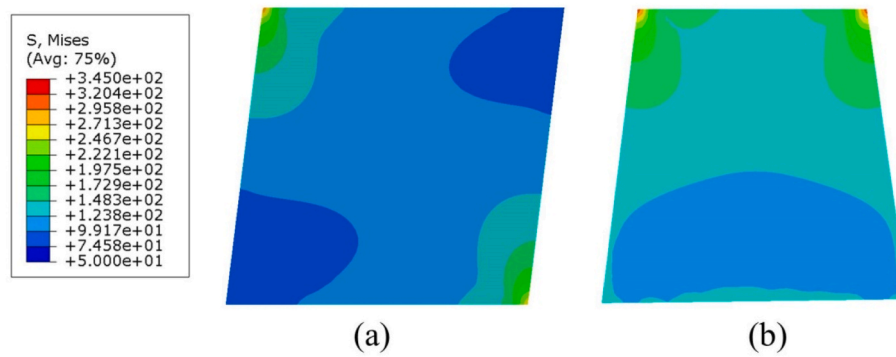


Fig. 13. Von Mises stress contours of the cross section of (a) 8° inclined cylindrical specimen and (b) cone specimen.

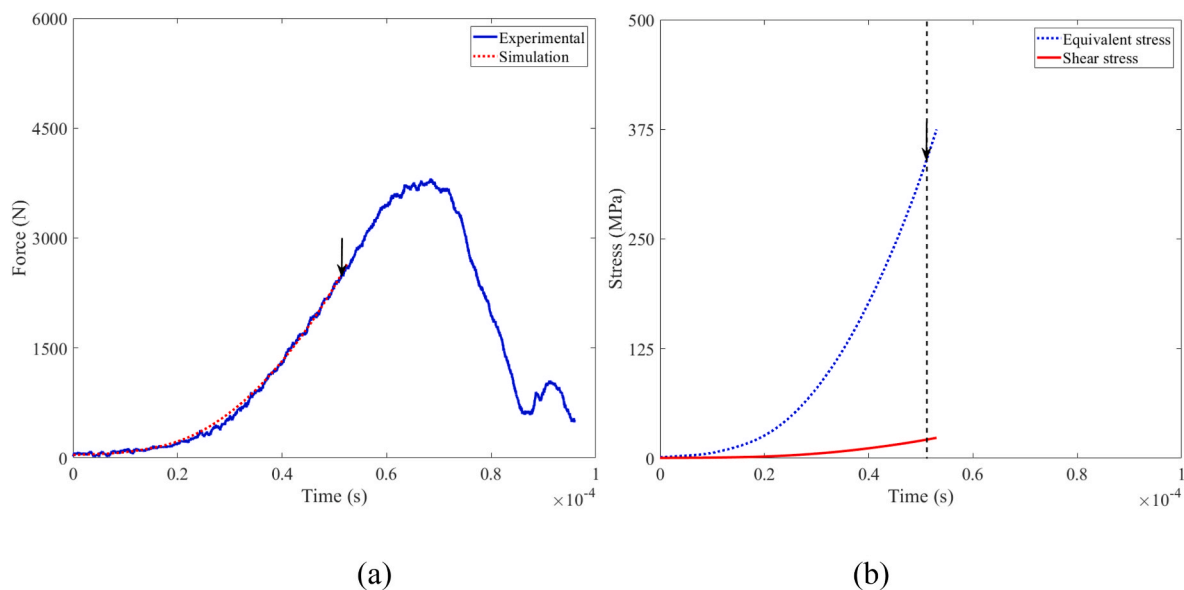


Fig. 14. Procedure to obtain the equivalent stress and shear stress of Macor at the initiation of failure (a) Global force history (b) Local stress histories.

state drives the crack propagating parallel to the inclined surface of the cone specimen. The fracture surface of ceramic materials under dynamic shear loading mode is rarely reported. The fractographic analysis in Fig. 11 shows the mica phase-cleavage plane zone and the compacted zone in the shear fracture surfaces of the inclined cylindrical specimen and the cone specimen. In the punch shear test of Bao et al. [42], the fracture surface of the ceramic showed similar comminution arising from the abrasion of the shear failure zones. The comminution also occurred in the Hertzian cone of various ceramics under impact [5–7]. These observations indicate the significant role of shear loading in the dynamic failure process of Macor.

The stress states of the inclined cylindrical specimen and the cone specimen can be determined, with the combination of finite element simulation, the SHPB analysis and the high speed photograph. Note that the linear elastic model shows the simplest phenomenological nature of Macor upon the damage initiation. This is consistent with the linear elastic part in the Johnson–Holmquist-II (JH-2) model [45]. The stress state right upon the initiation of damage is the main concern in this work, consequently, the linear elastic model is used to simulate the Macor ceramic. The JH-2 model used by Wang et al. [44] and Zhang et al. [46], and the phase-field model introduced by Salvati [47], would be helpful to describe the damage evolution and failure process in the next phase of the study. Different shear stress states are applied to the Macor ceramic using the inclined specimen and cone specimen. As shown in Fig. 15, the increase of shear stress reduces the equivalent

stress of Macor at the initiation of failure. With the similar obtuse angle corner (about 97–98°) and the shear stress component, the equivalent stress of the cone specimen is comparable to that of the 8° inclined cylindrical specimen. The cone specimen would also be a candidate to study the dynamic shear response of ceramic materials. As the Hertzian cone was formed in various ceramic materials under high speed impact (Townsend and Field [5,6]), the ceramic cone specimen would be able to provide further insight into the Hertzian cone failure process under impact. Note that the applied shear stress is relatively small in this work. A technique to directly introduce higher shear stress, see Bao et al. [42] or Cadoni et al. [56], will be considered in the next step. This is important to understand the degradation of equivalent stress of ceramic materials over a wide range of shear stress values.

Due to the opaque characteristic of Macor, the possible failure initiation inside the specimen cannot be observed from the high speed photographs. However, as the stress distribution is not uniform and the overall low stress remains inside the inclined cylindrical specimen or cone specimen, it is believed that the failure doesn't initiate from the inside of the specimens. Applying the current techniques to the transparent ceramic materials [57,58] and other advanced ceramic materials [59] would be of interest. The behaviour of Macor with zero porosity in the shear testing would be different from the behaviour of ceramic materials containing flaws such as porosity. As suggested by Louro et al. [9] and Savchenko et al. [60], the stress state and microstructural parameters affect the strength and impact damage of ceramics containing

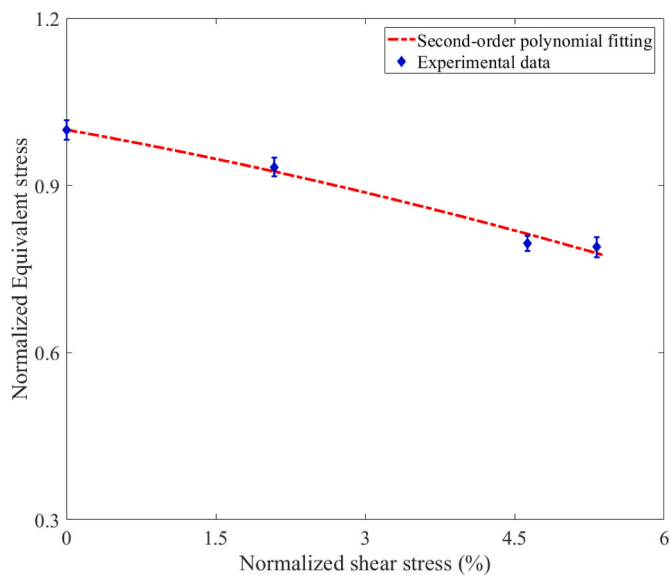


Fig. 15. Dynamic equivalent stress of Macor vs. shear stress at the initiation of failure. The stress values are normalized by the average equivalent stress of the cylindrical specimens, together with the standard error. The cylindrical specimen, 4° inclined cylindrical specimen, 8° inclined cylindrical specimen and cone specimen introduce a gradual increase of shear stress.

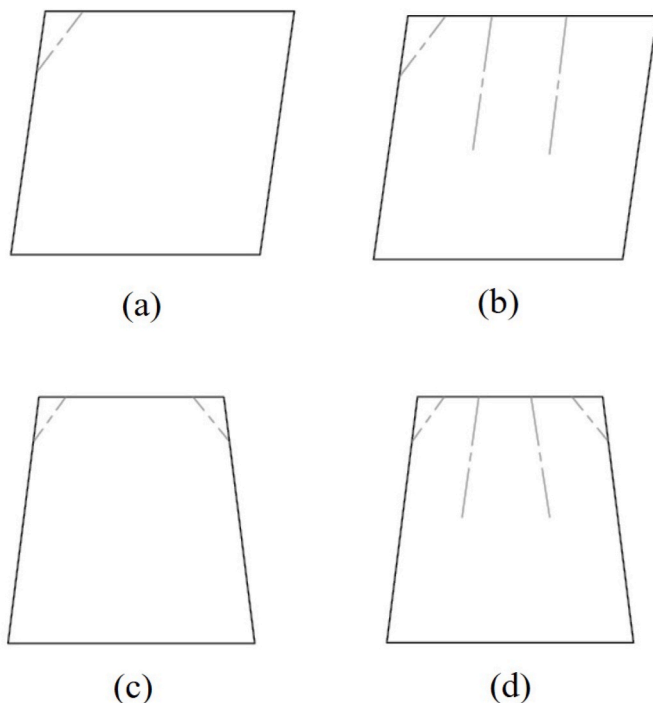


Fig. 16. Diagram of the failure process of the Macor specimens. The crack propagation is marked by the dashed line. (a) Splitting arising from the failure initiation of the inclined cylindrical specimen (b) Subsequent crack propagation of the inclined cylindrical specimen (c) Splitting arising from the failure initiation of the cone specimen (d) Subsequent crack propagation of the cone specimen.

flaws. The shear stress state would influence the growth and coalescence of the defects, and influence the strength and the dynamic failure process. Future work will continue to extend the shear testing technique, and adopt the techniques for ceramic materials containing flaws.

5. Conclusion

This paper studies the dynamic shear response of ceramic materials, using Macor as a model material, due to its light weight characteristic and importance in engineering applications. The cone specimen and the cylindrical specimens with different tilting angles are tested, using the SHPB and high speed photography techniques. The main outcomes are:

- The shear stress introduced by the tilting angle superimposes the axial compressive stress, which allows the study of the effect of shear stress on the dynamic failure of Macor.
- The high speed photography technique is employed to monitor the damage initiation and failure process of Macor. When the Macor ceramic is subjected to dynamic uniaxial compression, the failure is initiated in a manner of axial splitting. This is associated with the crack propagation along the axial loading direction.
- For the inclined cylindrical specimen and the cone specimen, the damage firstly initiates from the obtuse angle corner of the inclined specimens and the two corners at the minimum cross-section of the cone specimen. This is followed by the crack propagation parallel to the inclined surface direction.
- The fractographic analysis shows the comminuted zone in the shear fracture surfaces of the inclined cylindrical specimens and the cone specimen. The shear loading significantly affects the dynamic failure process of Macor.
- The equivalent stress decreases nonlinearly with the increase of shear stress at the initiation of failure. This indicates the equivalent strength of Macor is very sensitive to the applied shear stress.
- The equivalent stress of the cone specimen is similar to that of the 8° inclined cylindrical specimen, at a comparable shear stress. The cone specimen can be used to study the dynamic shear failure of ceramic materials. This would provide further insight into the Hertzian cone failure under high speed impact.

CRediT authorship contribution statement

Longhui Zhang: Conceptualization, Investigation, Methodology, Software, Formal analysis, Visualization, Resource, Self-supervision, Data curation, Writing – original draft, Writing – review & editing.

Declaration of competing interest

The author declare that there are no known competing financial interests or personal relationships that could have appeared to influence the work reported in this paper.

Acknowledgements

The support and fruitful suggestion from Dr. D. Townsend are greatly appreciated. Prof. N. Petrinic is acknowledged for the gun for hunting ceramics in the laboratory. Likewise, the assistance from Mr. P. Tantrum is appreciated.

References

- [1] M. Bengisu, *Engineering Ceramics*, Springer Science & Business Media, 2013.
- [2] P. Greil, *Advanced engineering ceramics*, *Adv. Eng. Mater.* 4 (2002) 247–254.
- [3] I. Beckwith, C. Miller III, *Aerothermodynamics and transition in high-speed wind tunnels at NASA Langley*, *Annu. Rev. Fluid Mech.* 22 (1990) 419–439.
- [4] H.S. Maiti, *Transparent and machinable glass-ceramics*, in: *Handbook of Advanced Ceramics and Composites: Defense, Security, Aerospace and Energy Applications*, 2020, pp. 461–493.
- [5] D. Townsend, J.E. Field, *Investigation of the Impact Performance of Various Glass and Ceramic Systems*. Annual Report, July 1985–July 1986, Cavendish Lab., Cambridge Univ. (UK), 1987.
- [6] J.E. Field, Q. Sun, D. Townsend, *Ballistic impact of ceramics*, *Inst. Phys. Conf. Ser.* 102 (1989) 387–393.
- [7] S. Walley, *Historical review of high strain rate and shock properties of ceramics relevant to their application in armour*, *Adv. Appl. Ceram.* 109 (2010) 446–466.

- [8] N. Murray, N. Bourne, Z. Rosenberg, The dynamic compressive strength of aluminas, *J. Appl. Phys.* 84 (1998) 4866–4871.
- [9] L. Loro, M.A. Meyers, Effect of stress state and microstructural parameters on impact damage of alumina-based ceramics, *J. Mater. Sci.* 24 (1989) 2516–2532.
- [10] Z. Rosenberg, N. Brar, S. Bless, Dynamic high-pressure properties of AlN ceramic as determined by flyer plate impact, *J. Appl. Phys.* 70 (1991) 167–171.
- [11] B. Hopkinson, A method of measuring the pressure produced in the detonation of high explosives or by the impact of bullets, *Proc. R. Soc. Lond. Ser. A* 89 (1914) 411–413.
- [12] H. Kolsky, An investigation of the mechanical properties of materials at very high rates of loading, *Proc. Phys. Soc. B* 62 (1949) 676.
- [13] W. Chen, G. Ravichandran, Dynamic compressive behaviour of ceramics under lateral confinement, *J. Phys. IV* 4 (1994). C8-177-C178-182.
- [14] L. Zhang, D. Townsend, N. Petrinic, A. Pellegrino, Loading mode and lateral confinement dependent dynamic fracture of a glass ceramic macor, *J. Dynam. Behav. Mater.* 8 (2022) 255–272.
- [15] J. Duffy, J.D. Campbell, R.H. Hawley, On the use of a torsional split Hopkinson bar to study rate effects in 1100-0 aluminum, *J. Appl. Mech.* 38 (1971) 83–91.
- [16] L. Meyer, S. Manwaring, Critical adiabatic shear strength of low alloyed steel under compressive loading, in: *International Conference on Metallurgical Applications of Shock-Wave and High-Strain-Rate Phenomena, EXPLOMET85*, 1985, pp. 657–674.
- [17] L. Meyer, E. Staskewitsch, A. Burlibies, Adiabatic shear failure under biaxial dynamic compression/shear loading, *Mech. Mater.* 17 (1994) 203–214.
- [18] Z. Wei, J. Yu, J. Li, Y. Li, S. Hu, Influence of stress condition on adiabatic shear localization of tungsten heavy alloys, *Int. J. Impact Eng.* 26 (2001) 843–852.
- [19] D. Rittel, S. Lee, G. Ravichandran, A shear-compression specimen for large strain testing, *Exp. Mech.* 42 (2002) 58–64.
- [20] A. Dorogoy, D. Rittel, A. Godinger, Modification of the shear-compression specimen for large strain testing, *Exp. Mech.* 55 (2015) 1627–1639.
- [21] L. Zhang, D. Rittel, S. Osovski, Thermo-mechanical characterization and dynamic failure of near α and near β titanium alloys, *Mater. Sci. Eng., A* 729 (2018) 94–101.
- [22] L. Zhang, Thermo-mechanical characterization and dynamic failure of a CoCrFeNi high-entropy alloy, *Mater. Sci. Eng., A* 844 (2022) 143166.
- [23] L. Zhang, D. Townsend, A. Pellegrino, N. Petrinic, Pure shear plastic flow and failure of titanium alloys under quasi-static and dynamic torsional loading, *Mech. Mater.* 167 (2022) 104262.
- [24] L. Zhang, D. Townsend, N. Petrinic, A. Pellegrino, Measurement of pure shear constitutive relationship from torsion tests under quasi-static, medium, and high strain rate conditions, *J. Appl. Mech.* 88 (2021) 121003.
- [25] P. Del Linz, P.A. Hooper, H. Arora, Y. Wang, D. Smith, B.R.K. Blackman, J.P. Dear, Delamination properties of laminated glass windows subject to blast loading, *Int. J. Impact Eng.* 105 (2017) 39–53.
- [26] S. Daly, D. Rittel, K. Bhattacharya, G. Ravichandran, Large deformation of nitinol under shear dominant loading, *Exp. Mech.* 49 (2009) 225–233.
- [27] **MACOR Machinable Glass Ceramic**, in: **Corning Incorporated**.
- [28] R.M. Quinn, L.H. Zhang, M.J. Cox, D. Townsend, T. Cartwright, G. Aldrich-Smith, P.A. Hooper, J.P. Dear, Development and validation of a Hopkinson bar for hazardous materials, *Exp. Mech.* 60 (2020) 1275–1288.
- [29] P. Li, C. Siviour, N. Petrinic, The effect of strain rate, specimen geometry and lubrication on responses of aluminium AA2024 in uniaxial compression experiments, *Exp. Mech.* 49 (2009) 587–593.
- [30] Y. Deng, H. Chen, X. Chen, Y. Yao, Dynamic failure behaviour analysis of TiB₂-B₄C ceramic composites by split Hopkinson pressure bar testing, *Ceram. Int.* 47 (2021) 22096–22107.
- [31] Z. Wang, R. Li, W. Song, Dynamic failure and inelastic deformation behavior of SiC ceramic under uniaxial compression, *Ceram. Int.* 46 (2020) 612–617.
- [32] X. Zhang, J. Ning, L. Zhao, G. Yang, Experimental study on dynamic mechanical properties of Al₂O₃ ceramics, *Trans. Beijing Inst. Technol.* 24 (2004) 178–181.
- [33] S. Acharya, S. Bysakh, V. Parameswaran, A.K. Mukhopadhyay, Deformation and failure of alumina under high strain rate compressive loading, *Ceram. Int.* 41 (2015) 6793–6801.
- [34] K. Evers, S. Falco, N. Grobert, R.I. Todd, Nacre-like alumina with unique high strain rate capabilities, *J. Eur. Ceram. Soc.* 40 (2020) 417–426.
- [35] L. Zhang, D. Townsend, N. Petrinic, A. Pellegrino, Pressure and temperature dependent dynamic flow and failure behavior of PMMA at intermediate strain rates, *Int. J. Impact Eng.* 158 (2021) 104026.
- [36] L. Zhang, D. Townsend, N. Petrinic, A. Pellegrino, The dependency of compressive response of epoxy syntactic foam on the strain rate and temperature under rigid confinement, *Compos. Struct.* 280 (2022) 114853.
- [37] L. GmbH, Product-Manual for DaVis 8.3: Imaging Tools, LaVision GmbH Gottingen, 2015.
- [38] G.T. GRAY III, Classic split Hopkinson pressure bar testing, *ASM Handb.* 8 (2000) 462–476.
- [39] L. Pochhammer, On the velocity of propagation of small vibrations in an isotropic cylinder of infinite length, *J. Reine Angew. Math* 81 (1876) 324–336.
- [40] C. Chyung, Microstructures & Mechanical Properties of Mica Glass-Ceramics, *Electron Microscopy and Structure of Materials*, 1972, pp. 1167–1194.
- [41] W. Li, H. Yu, L. Liu, X. Yuan, H. Dong, H. Wu, Study on the dynamic constitutive relationship and fracture mechanism of fluorophlogopite glass-ceramic, *Eng. Mech.* 36 (2019), 241–247, 256.
- [42] Y. Bao, H. Zhang, Y. Zhou, Punch-shear tests and size effects for evaluating the shear strength of machinable ceramics, *Zeitschrift für Metallkunde* 95 (2004) 372–376.
- [43] V. Abaqus, 6.14 Documentation, Dassault Systemes Simulia Corporation, 2014, p. 651.
- [44] Z. Wang, P. Li, Dynamic failure and fracture mechanism in alumina ceramics: experimental observations and finite element modelling, *Ceram. Int.* 41 (2015) 12763–12772.
- [45] T.J. Holmquist, D.W. Templeton, K.D. Bishnoi, Constitutive modeling of aluminum nitride for large strain, high-strain rate, and high-pressure applications, *Int. J. Impact Eng.* 25 (2001) 211–231.
- [46] X. Zhang, S. Li, Z. Li, Numerical simulation of dynamic response of laminated glass subjected to blast load, *Acta Armamentarii* 39 (2018) 1379–1388.
- [47] E. Salvati, Residual stress as a fracture toughening mechanism: a Phase-Field study on a brittle material, *Theor. Appl. Fract. Mech.* 114 (2021) 103021.
- [48] L. Zhang, A. Pellegrino, D. Townsend, N. Petrinic, Thermomechanical constitutive behaviour of a near α titanium alloy over a wide range of strain rates: experiments and modelling, *Int. J. Mech. Sci.* 189 (2021) 105970.
- [49] C.R. Siviour, S.M. Walley, Inertial and Frictional Effects in Dynamic Compression Testing, *The Kolsky-Hopkinson bar machine*, Springer, 2018, pp. 205–247.
- [50] X. Nie, W.W. Chen, X. Sun, D.W. Templeton, Dynamic failure of borosilicate glass under compression/shear loading experiments, *J. Am. Ceram. Soc.* 90 (2007) 2556–2562.
- [51] W. Chen, G. Ravichandran, Dynamic compressive failure of a glass ceramic under lateral confinement, *J. Mech. Phys. Solid.* 45 (1997) 1303–1328.
- [52] L. Farbaniec, J.D. Hogan, K.Y. Xie, M. Shaeffer, K.J. Hemker, K.T. Ramesh, Damage evolution of hot-pressed boron carbide under confined dynamic compression, *Int. J. Impact Eng.* 99 (2017) 75–84.
- [53] N. Bagdassarov, Viscoelastic behaviour of mica-based glass-ceramic aggregate, *Phys. Chem. Miner.* 26 (1999) 513–520.
- [54] B.R. Lawn, N.P. Padture, H. Cai, F. Guiberteau, Making ceramics" ductile, *Science* 263 (1994) 1114–1116.
- [55] Y. Xu, F. Dai, Dynamic response and failure mechanism of brittle rocks under combined compression-shear loading experiments, *Rock Mech. Rock Eng.* 51 (2018) 747–764.
- [56] E. Cadoni, M. Dotta, D. Forni, G. Riganti, Dynamic response of UHPFRcs in direct-shear tests, *Procedia Struct. Integr.* 28 (2020) 933–942.
- [57] L.B. Kong, Y. Huang, W. Que, T. Zhang, S. Li, J. Zhang, Z. Dong, D. Tang, *Transparent Ceramic Materials*, Transparent Ceramics, Springer International Publishing, Cham, 2015, pp. 29–91.
- [58] M.Z. Sheikh, Z. Wang, B. Du, T. Suo, Y. Li, F. Zhou, Y. Wang, U.A. Dar, G. Gao, Y. Wang, Static and dynamic Brazilian disk tests for mechanical characterization of annealed and chemically strengthened glass, *Ceram. Int.* 45 (2019) 7931–7944.
- [59] C. Dancer, J. Spawton, S. Falco, N. Petrinic, R. Todd, Characterisation of damage mechanisms in oxide ceramics indented at dynamic and quasi-static strain rates, *J. Eur. Ceram. Soc.* 39 (2019) 4936–4945.
- [60] N. Savchenko, I. Sevostyanova, T. Sablina, L. Gömze, S. Kulkov, The influence of porosity on the elasticity and strength of alumina and zirconia ceramics, in: *AIP Conference Proceedings*, American Institute of Physics, 2014, pp. 547–550.